Influences of wave directionality on a generic point absorber.

Jean-Christophe Gilloteaux and John Ringwood.

Department of Electronic Engineering,
National University of Ireland Maynooth,
Maynooth, Co. Kildare, Ireland
Email: jc.gilloteaux@eeng.nuim.ie

Abstract

The present study deals with the influences of wave directionality on a generic point absorber. The work presented here, shows how the dynamic of axisymmetric wave energy converter can be affected when one consider a realistic wave spectrum. For this purpose a non linear numerical model was used. The fluid structure interactions are modelled by means of a bending method where the Froude-Krylov forces are non linear and the radiation-diffraction problem is solved by using a linear method. Mooring loads are modelled via a finite element method. A compliant catenary mooring system composed by 4 mooring lines is hence used. Different models of sea spectra are used to approximate a real sea spectrum. The differences between them are discussed and comparisons on the body motions are commented.

Keywords: Point absorber, wave energy, random sea, mooring system.

1 Introduction

This paper focuses on wave directionality and its influence on the dynamic performances of a generic point absorber. A point absorber is optimized for efficient energy conversion. The resonant characteristic frequency of the system is at all times tuned to the characteristic frequency of the wave. Without caring any control system, wave energy developers have basically to match the peak frequency of the sea spectrum to the natural frequency of their device. This task could be easier if the frequency distribution of a sea state consist into a simple single peak spectrum but usually the corresponded spectrum is composed by several peaks of frequency (cf. Fig. 2) and is directional dependant. Moreover, as explained in [1], most of sea-states are composed by two or more superimposed wave systems which are time dependant. Although, for practical reasons, one usually uses single peak spectrum for modelling a specific sea state.

Regarding the incident wave train, five different spectral models were used to approximate a real sea-state. First of all, a single peak spectrum was used to take into account the specific frequency distribution of the wave train. As low frequency waves may propagate faster than the wind waves, a swell component is usually added to the locally wind sea creating multiple, or at least double, peak spectra. Hence, a double peak spectrum was used in order to have both swell and wind sea waves regarding the frequency distribution. In a second step, a spreading function was added to both single and double-peaked spectra in order to take into account the directional dependence. Generally sea states are composed by more than one swell component and one wind wave component, that's why a real directional wave spectrum was also considered. For this task, a numerical procedure was developed to fit this real 2D wave spectrum allowing the representation of simultaneous systems.

The purpose of the present study is to assess how the results are influenced according to the spectral model used and whether the body motions can be affected by parametric instabilities which may arise when a more precise model than the single-peaked one is applied. A non linear time-domain hydrodynamic model is used for modelling the hydrodynamic loads. The Froude-Krylov forces are computed on the instantaneous and exact wetted surface whereas the diffraction-radiation problem is solved by means of the boundary element method (BEM) code ACHIL3D [5]. Mooring loads are computed by using a finite element method modelling a compliant catenary system composed by four mooring lines. Comparisons regarding the body dynamics are shown where the heave, roll, pitch and yaw motions are examined.

2 Generic point-absorber

1. Geometry and dimensions

A generic point absorber is considered for the purpose of this study. The body is a generic point absorber represented as a truncated vertical cylinder with a diameter *D* and a draft *d*. Its dimensions were chosen to have a natural heave frequency equal to the peak frequency of the current sea state.

The natural heaving frequency of a floating body is

$$f_z = \frac{1}{T_z} = \frac{\omega_z}{2\pi} = \frac{1}{2\pi}\sqrt{\frac{K_{33}}{(m+m_w)}} \quad (1)$$

According to McCormick [2], the theoretical added mass expression m_W for such a floating circular cylinder is the following:

$$m_w = \rho\frac{D^3}{6} \quad (2)$$

We also know that the hydrostatic stiffness term K_{33} is as follow

$$K_{33} = \rho g \pi \frac{D^2}{4} \quad (3)$$

So, using Eq.(2) and Eq.(3) we may write Eq. (1) as

$$f_z = \frac{1}{2\pi}\sqrt{\frac{\rho g \frac{\pi D^2}{4}}{\rho\pi\frac{D^2}{4}d + \rho\frac{D^3}{6}}} \quad (4)$$

As a point absorber is considered like a system in which the horizontal extent is much smaller than one wavelength, the radius was imposed. This latter assumption permits us to determine the best value regarding the draft *d* and to obtain the following:

$$d = \frac{g}{\omega_z^2} - \frac{2D}{3\pi} \quad (5)$$

2. Body dynamics

We have allowed the three-dimensional device to undergo arbitrary six-degrees-of-freedom motions. In a first step we define an initial inertial frame of reference R_0 linked to the physical space, assimilated to a Galilean referential. The origin O of this referential is fixed to the center of mass of the body at the initial time. A rigid motion moving R_0 to a new referential Rb is then carried out to place the body in space.
The Newton's second law leads to the two Eqs. (6) and (7), where G is the center of gravity of the system, f_{bG} the total force acting on the body and M_{bG} the torque.

$$m\left(\dot{v}_G^b + \dot{\Omega}_{0b}^b \times v_G^b\right) = f_G^b \quad (6)$$

$$I_G\dot{\Omega}_{Ob}^b + \Omega_{Ob}^b \times I_G\Omega_{Ob}^b = m_G^b \quad (7)$$

Eq. (6) corresponds to the translation motion of the centre of gravity in body-fixed coordinates and Eq. (7) describes the attitude dynamics of the body in the body-fixed frame. The body orientation has been described by using a quaternion $Q=[q_0, q_1, q_2, q_3]$.

In vectorial settings Eqs. (1) and (2) may be expressed as

$$\mathbf{M}\mathbf{v} + \boldsymbol{\tau}_{Coriolis} = \boldsymbol{\tau}$$

Where

- $\mathbf{v} = \left[v_G^b, \Omega_{Ob}^b\right] = [u, v, w, p, q, r]^T$ is the generalized velocity vector decomposed in the body-fixed frame.
- **M** the inertia matrix.
- $\boldsymbol{\tau}_{Coriolis}$ the Coriolis forces.
- $\boldsymbol{\tau} = \left[f_G^b, m_G^b\right] = [X, Y, Z, K, M, N]^T$ is the generalized vector of external forces and moments. $\boldsymbol{\tau}$ is composed by the pressure forces due to the fluid-structure interactions, and the mooring loads.

Therefore, using Eqs. (1) and (2) the motion decomposition leads to the following coupled system

$$\begin{bmatrix} m & 0 & 0 & 0 & 0 & 0 \\ 0 & m & 0 & 0 & 0 & 0 \\ 0 & 0 & m & 0 & 0 & 0 \\ 0 & 0 & 0 & I_{xx} & I_{xy} & I_{xz} \\ 0 & 0 & 0 & I_{yx} & I_{yy} & I_{yz} \\ 0 & 0 & 0 & I_{zx} & I_{zy} & I_{zz} \end{bmatrix} \frac{d}{dt}\begin{bmatrix} u \\ v \\ w \\ p \\ q \\ r \end{bmatrix} + \begin{bmatrix} m(-vr+wq) \\ m(-wq+ur) \\ m(-uq+ur) \\ (I_{zz}-I_{yy})qr \\ (I_{xx}-I_{zz})rp \\ (I_{yy}-I_{xx})pq \end{bmatrix} = \begin{bmatrix} X \\ Y \\ Z \\ K \\ M \\ N \end{bmatrix} \quad (8)$$

$$\frac{d}{dt}\begin{bmatrix} x \\ y \\ z \end{bmatrix} = \begin{bmatrix} u \\ v \\ w \end{bmatrix} \quad (9)$$

$$\frac{d}{dt}\begin{bmatrix} q_0 \\ q_1 \\ q_2 \\ q_3 \end{bmatrix} = \frac{1}{2}\begin{bmatrix} 0 & -p & -q & -r \\ p & 0 & r & -q \\ q & -r & 0 & p \\ r & q & -p & 0 \end{bmatrix}\begin{bmatrix} q_0 \\ q_1 \\ q_2 \\ q_3 \end{bmatrix} \quad (10)$$

$$q_0^2 + q_1^2 + q_2^2 + q_3^2 = 1 \quad (11)$$

Eq. (8) corresponds to the Newton's second law, Eqs. (9) and (10), giving the generalised velocity components of the body. Eq. (9) gives the translation displacement and Eq. (10) the rotational motion. Eq. (11) is redundant because a quaternion rotation has always a unit length. However, the numerical resolution of Eq. (10) does not maintain precisely this length and a renormalization is then necessary.

3. Fluid-structure interactions

In this paper we used a time-domain non-linear potential-flow method. The fluid is considered homogeneous, incompressible, inviscid and with an irrotational flow. Surface tension is not taken into

account and the depth is considered infinite and a linearized free surface and body boundary conditions are used.
This method is particularly useful for the prediction of large-amplitude motions for single or multi-body devices in a prescribed or arbitrary sea state [3] and [4]. The fluid forces acting on the body can be non-linear with respect to certain motion variables, e.g. the quadratic component of the Bernoulli's equation. Froude-Krylov forces contain "geometric" non-linearities as the forces are computed by integrating over the exact instantaneous position and wetted surface.

- Froude-Krylov forces

The Froude-Krylov forces are the loads introduced by the unsteady pressure field generated by undisturbed waves. In this model, the Froude-Krylov forces are completely nonlinear. The pressure of the incident wave-train is integrated on the instantaneous wetted-surface *S(t)* defined by the intersection between the non-disturbed incident free-surface and the shifted floating body, as follow

$$F_{FK}(t) = \iint_{S(t)} \left(P_{stat}(t) + P_{dyn}(t) \right) \mathbf{n}(t) dS \tag{12}$$

with

$$\begin{cases} P_{stat} = -\rho g z \\ P_{dyn} = -\rho \dfrac{\partial \phi_I}{\partial t} - \rho \dfrac{\nabla \left| \phi_I \right|^2}{2} \end{cases} \tag{13}$$

Where P_{stat} and P_{dyn} are the hydrostatic pressure and the dynamic pressure, respectively. **n** corresponds to the normale of the wetted surface *S(t)* and ρ to the water density.
The pressure of the incident wave field ϕ_I is, for this study, derived from Airy wave theory.
A robust geometry processing is essential for large amplitude motions. Consequently, an automatic remeshing routine is used for this task. At each time step, the underwater geometry is represented by a number of panels. As the body moves, its new location and orientation are updated in the global coordinate system and the new waterline is found from the intersection with the instantaneous free surface. The underwater portion of each panel is then repanelized using the transfinite method.

- Radiation forces

The radiation forces are the hydrodynamic forces associated with the motion of the floating body. The linear radiation forces have been expressed as a convolution product according to the well-known Cummins' decomposition

$$F_{rad}(t) = -\boldsymbol{\mu}_\infty v(t) - \int_0^t \mathbf{K}\left(t-\tau\right) \mathbf{v}(\tau) d\tau \tag{14}$$

where $\boldsymbol{\mu}_\infty$ is the added masses matrix and **K** the impulse response function for the radiation forces which are previously computed by the BEM code ACHIL3D.

It can be first transformed in order to remove the convolution product by using Prony's method [6]. This method has been developed by Clément for the computation of impulse response of radiation forces. This method computes couples of variables (α_i, β_i) defining the following approximation of the real function **K** of the Eq. (14)

$$K_{ij}(t) \approx \sum_{m=1}^{N_{ij}} \alpha_{ijm} \exp^{\beta_{ijm} t} \tag{15}$$

K being a real function, either (α_i β_i) are real, either they are complex and systematically associated with their complex conjugates. So, if

$$I_{ij}(t) \approx \int_0^t K_{ij}\left(t-\tau\right) \mathbf{v}\left(\tau\right) d\tau \tag{16}$$

the computation of the convolution product in the equation gives the following result

$$\begin{cases} \tau_{rad}(t) = -\boldsymbol{\mu}_\infty v\left(t\right) - \mathbf{I} \\ \dot{\mathbf{I}} = \beta \mathbf{I} + \alpha v \end{cases} \tag{17}$$

- Diffraction forces

The diffraction forces are associated with the disturbance introduced into the wave system by the presence of the floating body. Like the radiation forces, the diffraction forces are based here on linear time-domain theory. The diffracted wave forces are computed as

$$F_{diff}(t) = \int_{-\infty}^{+\infty} \mathbf{K}_7\left(t-\tau\right) \eta\left(\tau\right) d\tau \tag{18}$$

where η is the free-surface elevation of the incident-wave train at a given reference point and $\mathbf{K}_7$ the impulse response function for the diffraction forces given by ACHIL3D.

The reader is referred to [7] for further details concerning the hydrodynamic model.

4. Mooring loads

A passive station-keeping system is taken into account in this study for counteracting the horizontal environmental forces so that the wave energy device remains within specified position tolerances. Hence, in the same time, the system must be compliant enough to allow the wave frequency motion and must transfer the resulting horizontal forces to the seabed. To ensure those properties, a multi-point compliant catenary mooring system is used (cf. Fig. 1).

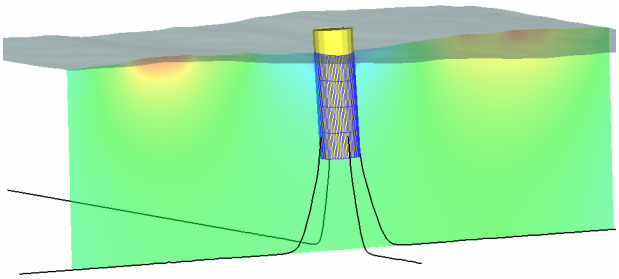

Figure 1: Mooring system arrangement.

As optimal mooring configuration for a point absorber is beyond the scope of this study, we have chosen a typical configuration, usually used for offshore structures and especially for SPAR platforms [8]. Hence, a 4 lines mooring system has been chosen.

A finite element method (FEM) was used to model the mooring lines. As in [9], it solves the equation of motion of a cable with negligible bending and torsonial stiffness given by the following equation:

$$\rho_{CL}\frac{\partial\vec{\mathbf{v}}(t,s)}{\partial t}=\frac{\partial}{\partial s}T\left((t,s)\vec{\mathbf{t}}(t,s)\right)+\vec{\mathbf{f}}(t,s)\left(1+e(t,s)\right) \quad (19)$$

where s, **v** and **t** are, respectively, the distance along the unstretched cable, velocity and tangential vector. ρ_{CL} is the mass per unit length of the unstretched cable, T the tension, e the strain and **f** the sum of the external loads acting on the cable.

According to Hooke's law we may get

$$\rho_{CL}\frac{\partial^2\vec{\mathbf{r}}(t,s)}{\partial t^2}=\frac{\partial}{\partial s}\left(EA\frac{e}{1+e}\frac{\partial\overrightarrow{\mathbf{r}(t,s)}}{\partial s}\right)+\vec{\mathbf{f}}(t,s)(1+e) \quad (20)$$

with E is the young's modulus, A the cross sectional area of the cable and **r** the position vector.
The external forces term **f** gathers the hydrostatic and hydrodynamic forces acting on the cable plus the gravity as follow:

$$\vec{\mathbf{f}}=\overrightarrow{\mathbf{f}_S}+\vec{\mathbf{f}}_{D_n}+\vec{\mathbf{f}}_{D_t}+\vec{\mathbf{f}}_{FK} \quad (21)$$

The effect of gravity on the mass of the cable leads to:

$$\vec{\mathbf{f}}_S=\rho_c A_C\vec{\mathbf{g}} \quad (22)$$

with ρ_c is the density of the cable and **g** the gravitational acceleration.

The formulation for the hydrodynamic drag forces is derived from the so-called Morison's equation

$$\vec{\mathbf{f}}_{D_n}=-\frac{1}{2}C_{D_n}d\rho_w\left|\vec{v}_n\right|\vec{v}_n \quad (23)$$

$$\vec{\mathbf{f}}_{D_t}=-\frac{1}{2}C_{D_t}d\rho_w\left|\vec{v}_t\right|\vec{v}_t \quad (24)$$

where C_{Dn} and C_{Dt} are, respectively the normal and tangential drag coefficients for the cable. d is the diameter of the cable and ρ_w the density of the water. The Froude-Krylov forces include the buoyancy effect plus the effect due to the acceleration of the fluid $\mathbf{a_w}$:

$$\vec{\mathbf{f}}_{FK}=\rho_w A_C\left(-\vec{\mathbf{g}}+\vec{\mathbf{a}}_w\right) \quad (25)$$

3 Random sea modelling

Data from Monterey Bay in California (station 46042) and provided by the National Data Buoy Center (NDBC) were used. Two-dimensional spectra and standard meteorological data over a year (January-December 2007) have been collected with a sampling period about 1 hour. For the present study only one sea state is considered with the properties given in Table 1. Usually parametric spectra are used for representing sea-states. Scatter diagrams are provided for many different locations around the world giving the peak frequencies and the significant wave heights from past years. However those data don't provide any information about the shape of the spectrum, that's why we have chosen the spectrum of Fig. 2. Indeed, this spectrum has three main frequency peaks which cannot be well fitted by the common parametric spectra. As this kind of spectrum is not rare in the nature, it is a good example for assessing the influence of the sea-state description on a generic wave energy device.

H_S	T_P	θ_m
2.68 m	10.81s	314°

Table 1: Sea state properties.

For this purpose, we decided to model the current sea-state by means of five different spectral models. The two first models use standard one-dimensional spectrum to which a directional spreading function was added in order to take into account the directional dependence of the wave propagation. Then, a numerical method, called partitioning method, was used which is able to represent sea-states composed by many simultaneous wave systems. Those models are as follows:

- Frequency spread.

The choice of the spectral models was carried out by comparing, for both 1D and 2D spectra, the most popular ones and by choosing the one which best fits the real spectrum regarding the mean squared error. Hence, for the single peak spectrum we have compared the JONSWAP spectrum with the Bretschneider spectrum (also known as the Modified Pierson-Moskowitz spectrum). Considering the double peak spectrum, the Ochi-Hubble spectrum was compared to the Torsethaugen spectrum. For the current sea state, Fig. 2 shows that the Bretschneider spectrum and the Ochi-Hubble spectrum seem to be the more relevant models to approximate the real spectrum. These results are in accordance to [10] and seem consistent as both Bretschneider spectrum and Ochi-Hubble spectrum were developed by using the same data set.

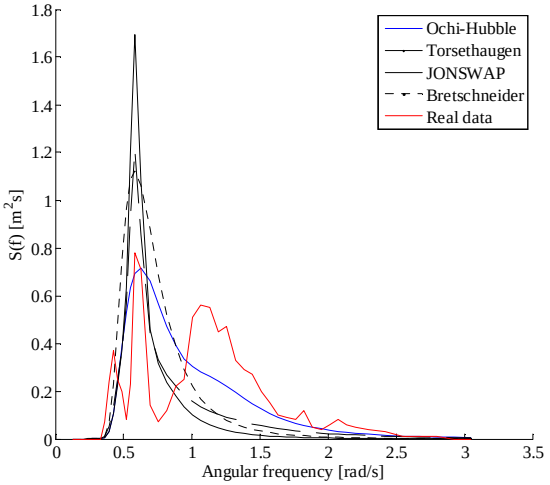

Figure 2: Spectral models and real data.

- Directional spread.

For the purpose of the directional spread, the directional wave spectrum *DWS* is assumed to be composed by a parametric spreading function $D(f,\theta)$ is that the directional spectrum is described by

$$DWS(f,\theta) = S(f).D(f,\theta) \tag{26}$$

where $S(f)$ is the one-dimensional energy spectral density function, f and θ being the frequency and the direction.

The direction spreading function can be modeled using a variety of parametric models [11]. Due to specifications of sites, no single model is universally accepted. Here the angular spreading function used is the cosine power '2s' model describes as follows:

$$D(f,\theta) = G(s)\cos^{2s}\left[\frac{(\theta-\theta_m)}{2}\right] \tag{27}$$

where,

$$G(s) = \frac{2^{2s-1}}{\pi}\frac{\Gamma^2(s+1)}{\Gamma(2s+1)} \tag{28}$$

is defined such as

$$\int_{-\pi}^{\pi} D(f,\theta)d\theta = 1 \tag{29}$$

where Γ is the Gamma function, θ_m the mean wave direction and s the spreading parameter which is, a priori, a function of frequency and wind speed.

This spreading function was proposed by Longuet-Higgins & al. [12]. Here the value of the parameter 's' controls directional spreading around the mean wave direction.

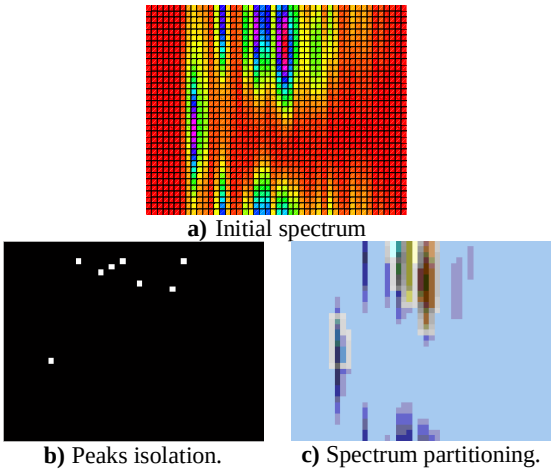

a) Initial spectrum

b) Peaks isolation. **c)** Spectrum partitioning.

Figure 3: Stages in the segmentation process.

- Partitioning method

For the purpose of extracting all the significant wave systems from the real 2D spectrum, a numerical method has been developed in Matlab by means of the image processing toolbox. An approach similar to [1] was used where the process can be divided into three stages: spectrum segmentation, wave system identification, and analytical fitting.

Spectrum segmentation

This stage aims to catch all the spectral regions associated to a local peak of energy. First of all, an energy threshold is used to avoid any non relevant peak of energy [13]. The 2D spectrum is then converted into intensity image in order to find the regional maxima. The intensity image is then modified by using morphological reconstruction and by superposing the regional maxima with the image. This is done to facilitate the computation of the boundaries of the regional maxima performed by a watershed method as in [14] which determines the boundaries of each area containing a peak of energy (Fig. 3).

Wave system identification

The purpose of this stage is to locate wind sea peaks from swell peaks (cf. Fig. 4 and table 2). As in [15], wind sea and swell are identified regarding the separation frequency f_S:

$$f_s = \frac{g}{\beta 2\pi U_W\left|\cos(\theta_W-\theta_m)\right|} \tag{30}$$

where g is the acceleration of gravity, U_W the wind speed and θ_W the wind direction. Thus, a peak is classified as wind sea if:

$$\begin{cases} f_P > f_S \\ \left|\cos(\theta_W-\theta_m)\right| \le \dfrac{\pi}{2} \end{cases}$$

Once every sea system are identified, neighboring swell and wind sea peaks that belong to the same swell or wind sea system are considered mutual and are combined. Thus, two sea systems are considered mutual if they satisfy the both following conditions:

$$\left[\theta_{p,1}-\theta_{p,2} \le \kappa_\theta\right] \cap \left[f_{p,1}-f_{p,2} \le \kappa_f\right] \tag{31}$$

Where θ_p is the peak direction and $[\kappa_\theta, \kappa_f]$ are spread factors adjusted to optimize performance of the partitioning process.

Analytical fitting

An analytical fitting process is performed in the least square sense in order to have a parametric representation of the real sea spectrum. The directional wave spectrum is modeled as in Eq.(19) with the cosine 2s spreading function (Eq.(20)) for the directional spreading and with a JONSWAP spectrum for the one-directional wave spectrum $S(f)$:

$$S(f) = \alpha\frac{g^2}{(2\pi)^4}\left(\frac{f}{f_P}\right)^{-5} e^{-\frac{5}{4}\left(\frac{f}{f_P}\right)^{-4}} \gamma^{e^{\left[\frac{(f-f_P)^2}{2\sigma^2}\right]}}$$

With

	1	2	3	4	5	6	7	8
type	wind sea	wind sea	wind sea	wind sea	wind sea	wind sea	swell	swell
$\theta_m(^o)$	329.1	308.5	329.1	288	277.7	329.1	144	143.7
ω_P(rad/s)	0.93	1.18	1.37	1.6	1.78	2.03	0.44	0.6

Table 2: Characteristics of each wave system extracted by the partitioning method.

$$\alpha \mid H_S = \sqrt{\int_0^\infty S(f)df} \tag{32}$$

and

$$\begin{cases} \sigma = 0.07 \text{ for } f \le f_P \\ \sigma = 0.09 \text{ for } f > f_P \end{cases} \tag{33}$$

This fitting process is carried out into two steps. The first step consists of using the cosine 2s function and of finding the best set [s,θ_m] to fit the real spectrum in the least square sense for the directional distribution. Then, the second step uses the set [α, f_P, γ] which is iteratively computed in order to find the best values for fitting the real spectrum regarding the frequency distribution.

Finally, an overlap correction is carried out for each wave system. Indeed, each wave sea system extracted may overlap the surrounding sea system. So, for each sea system, a correlation matrix is computed with its neighborhood providing a correction factor.

Computation of Froude-Krylov and diffraction forces

The random wave is modeled as a linear superposition of a large number of elementary Airy waves with amplitudes related to the wave spectrum.

After sampling the directional wave spectrum into equally spaced directions and into equally spaced frequencies, the amplitude *a* of each component of the wave of angular direction θ and frequency *f* is selected randomly via a Rayleigh distribution with root mean square *rms* as mentioned in [16] equal to

$$rms = \sqrt{2S(f)D(f,\theta)\Delta f \Delta\theta} \tag{34}$$

either with the Bretschneider spectrum, or with the Ochi-Hubble spectrum.

Then, as the incident wave train is modeled as a linear superposition of monochromatic waves, one can synthesize a representative sample of the waves for a sea state defined by the couple (H_S,T_P) by using

$$\eta(x,y,t) = \sum_{i=1}^{N_\theta}\sum_{j=1}^{N_w} a\left(\frac{w_j}{2\pi},\theta_i\right) \cos\left(k_j\left(x\cos\theta_i + y\cos\theta_i\right) - w_j t + \varphi_{ij}\right) \tag{35}$$

where η is the free surface elevation and w_j the angular frequency of the jth wave component for one angular direction. φ_{ij} represents the phase uniformly distributed on the interval [0,2π] as an independent stochastic variable.

As it is a linear approach, the total velocity potential of the incident wave-train ϕ_I used in Eq. (9) is expressed as a linear superposition of elementary potentials of each component. Hence, for each direction and each frequency a velocity potential is associated as follow

$$\phi_I(x,y,t) = \sum_{i=1}^{N_\theta}\sum_{j=1}^{N_w} a\left(\frac{w_j}{2\pi},\theta_i\right)\frac{ch\,k(z+h)}{ch\,k(h)} \sin\left(k_j\left(x\cos\theta_i + y\cos\theta_i\right) - w_j t + \varphi_{ij}\right) \tag{36}$$

As for the velocity potential, the total diffraction is expressed as a linear superposition of elementary forces. Indeed, ACHIL3D computes for each direction an associated impulse response function K_{7i}. So, the total diffraction force is expressed as

$$F_{diff}(t) = \sum_{i=1}^{N_\theta} K_{7i}(t-\tau)\eta_i(\tau)d\tau \tag{37}$$

4 Results

Different models were used to simulate the same sea-state. For each simulation, the point absorber has six degrees of freedom. Fig. 5 shows the motions of a moored point absorber in random waves. Results for different spectral models with same statistical properties (*Hs*, T_P) are presented in Fig. 5.

Single peak spectrum was used by using a Bretschneider spectrum and double peak spectrum via a Ochi-Hubble spectrum. Then, a spreading function was added to both of them in order to take into account the wave directional properties. Finally, by means of a partitioning method, we have modeled the incident wave train by taking into account simultaneous swell and wind sea systems (cf. Fig. 4) approximating the bidimensional real spectrum provided by NDBC.

For each model, one simulation about 300s was launched. The equations of motion formulated using quaternion Eqs. (8) to (10) are solved using a fourth-order Runge-Kutta (RK4) method with a time step dt=0.01s.

The body dimensions were chosen in order to have a natural period in heave about 10.81s (corresponding to the peak period of the current sea state), by using Eq. (5). The resulting dimensions are: a diameter *D* is equal 10 m and a draft *d* is equal to 27 m.

Concerning the mooring system, a water depth about 50 m was assumed. According to Fitzgerald [17], the length of each line was fixed to 250 m in order to have a ratio between the length and the water depth (also called the scope) equal to 5. The mooring lines properties (Table 3) were chosen according to [18].
For the random wave modelling, each directional spectrum was sampled into 180 equally spaced directions ($\Delta\theta$=2°) and each one-directional wave spectrum into 225 equally spaced frequencies (Δf=0.01 rad/s). The value of the spreading parameter for both the 2D Bretschneider spectrum and the Ochi-Hubble spectrum was set to s=12 as it is the common value used for practical purposes [11].

Regarding the spectral models, the results show that even when one takes into account the influences of the wind, some peak frequencies may missed regarding the real frequency spectrum (cf. Fig. 2). So, it means that the natural frequency of the body tuned regarding the peak frequency may not longer be optimal for this sea state.

About the body motion, the results show (Fig. 5) that, whatever spectral model, the dynamic behaviors are very close despite the fact that the sway, roll and yaw motions are exited when wave directionality is taken into. Nevertheless, it is clear that the directional spread has a bad influence on the performances. It denotes that whether a wave energy converter is only tuned by taking into account a one-directional wave spectrum, the performance may be overestimated.

Regarding the one-directional spectra, the results show that the influence of a double peak spectrum is not very relevant for the present generic point absorber. Indeed, the dynamic behavior is slightly the same with a Bretschneider spectrum or with a Ochi-Hubble spectrum. Nevertheless, when the directional spread is considered a different behavior is observed. The results show that pitch and roll amplitudes are larger for the Bretschneider spectrum than for the Ochi-Hubble spectrum. This phenomenon can be explained by the yaw motion which is larger with the Bretschneider spectrum. Indeed, regarding the yaw motion, it appears that the heaving buoy has a very long natural yaw period. It is linked to the small mooring stiffness which tends to give a very low frequency motion to the point absorber where the hydrodynamic damping is very small resulting in a very slow transient motion.

Length (m)	l	250
mass per unit length (Kg/m)	ρ_0	61
Density of the cable (Kg/m^3)	ρ_C	7800
Axial stiffness (MN)	EA	100
Normal drag coefficient	C_{Dn}	2.5
Tangential drag coefficient	C_{Dt}	0.5

Table 3: Mooring lines properties**.**

The results also show that the directional spread may significantly influence the behavior of the generic point absorber. As sway, roll, and yaw motions are involved for a bidimensional spectrum, it tends to reduce the motion amplitude of the heave and pitch. So despite its axisymmetric geometry, the generic point absorber moored to the sea bed via four compliant mooring lines tends to be directional dependent.

Finally, the last model using simultaneous wave systems (Fig. 6) shows that the behavior is slightly the same as for the previous spectral models. Nevertheless, the motion period is affected. Indeed the motion period with the real spectrum is about 7,5s whereas it was close to the peak period for both Bretschneider spectrum and Ochi-Hubble spectrum. This can result of the large number of peaks not taken into account with the previous models and which are present in the real bidimensional spectrum changing radically the excitation forces. It signifies that, regarding its natural period, the device is no longer optimal for this sea-state whereas it was optimal with the parametric models.

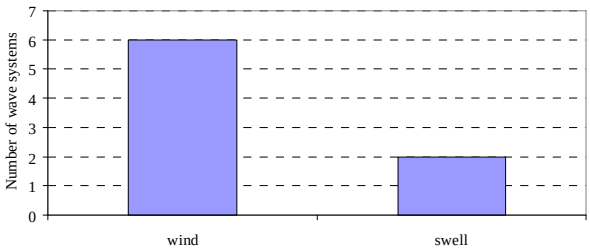

Figure 4: Number of simultaneous wind sea systems and swell systems.

Conclusions

The aim of this study is to show how the usual spectral models composed by a single peak spectrum may influence the performances of a moored generic point absorber.

Five different models were used in order to highlight the influence of the directional spread and of simultaneous wind sea and swell systems. The results show that the directional spread significantly affect the behavior of the generic point absorber as sway, roll and yaw motions are excited. It also shows that simultaneous sea systems may affect the behavior of a point absorber and that an accurate description of the sea state seems very useful to assess the performance of a wave energy device.

It also shows that mooring system may play an important role regarding the dynamic behavior of a point absorber. The present study only deals with a single device; however one has to keep in mind that even if a single device has a good behavior with an adapted mooring system, additional problems may occur for an array of devices with a completely different mooring system.

It also seems relevant to use a refined model to describe a sea state regarding the dynamic stability of wave energy devices. For instance parametric instabilities like parametric rolling may be found out when an accurate description of the sea state is used

coupled to a numerical model allowing a full description of the body dynamic.

Finally, it turns out that any device must be considered as a non directional device as soon as a mooring system embedded to the sea bed is used. However, in order to have a good picture of the influences that wave directionality has on a wave energy converter, a better investigation must be done. For instance, a computation over several years could be performed where comparisons on the absorbed power regarding the different models could be carried out. This is what we intend to do in the future.

Acknowledgements

The authors are grateful for the financial support provided by Enterprise Ireland.

References

[1] M.-A. Kerbiriou, M. Prevosto, C. Maisondieu, A. H. Clément, and A. Babarit, "Influence of sea-states description on wave energy production assessment." in *7th European Wave and Tidal Energy Conference*, 2007.

[2] M. E. McCormick, *Ocean Wave Energy Conversion*. John Wiley and Sons, 1981.

[3] J.-C. Gilloteaux, G. Bacelli, and J. Ringwood, "A non-linear potential model to predict large-amplitudes-motions: application to a multi-body wave energy converter." in *Proc. 10th WREC*, 2008.

[4] J.-C. Gilloteaux, A. Babarit, G. Ducrozet, M. Durand, and A. Clement, "A non linear potential model to predict large amplitude motions: application to the searev wave energy converter," *Pr. of the 26th Int. Conf. OMAE*, 2007.

[5] A. Clément, "Hydrodynamique instationnaire linéarisée : 'mise en oeuvre d'une méthode de singularités utilisant un modèle différentiel de la fonction de green.'," Laboratoire de Mécanique des Fluide de l'Ecole Centrale de Nantes, Tech. Rep. LHN-9703, 1997.

[6] G. Duclos, A. H. Clément, and G. Chatry, "Absorption of outgoing waves in a numerical wave tank using a self adaptive boundary condition," *Int J. Offshore Polar Engng*, vol. 11, no. 3, pp. 168–175, 2000.

[7] J.-C. Gilloteaux, "Simulation de mouvements de grande amplitude. application à la récupération de l'énergie des vagues." Ph.D. dissertation, Ecole Centrale de Nantes, 2007.

[8] X. Chen, J. Zhang, and W. Ma, "On dynamic coupling effects between a spar and its mooring lines." *Ocean Engineering*, vol. 28, pp. 863–887, 2001.

[9] O. Aamo and T. I. Fossen, "Finite element modelling of moored vessels," *Mathematical and Computer Modelling of Dynamical Systems*, vol. 7, pp. 47–75, 2001.

[10] B. Roger, "Oregon offshore wave power feasibility demonstration project, phase 1.5," EPRI, Tech. Rep., 2005.

[11] M. Tucker and E. Pitt, *Waves In Ocean Engineering*, O. E. Series, Ed. Elsevier Science Ltd, 2001, vol. 5.

[12] M. Longuet-Higgins and al, "Observations of the directional spectrum of sea waves using the motions of a floating buoy," *Journal of Physical Oceanography*, vol. 5, pp. 750–760, 1963.

[13] J. Hanson and O. Philips, "Automated analysis of ocean surface directional wave spectra," *Journal of Atmospheric and Oceanic Technology*, vol. 18, pp. 277–293, 2001.

[14] J. Hanson and R. Jensen, "Wave system diagnostics for numerical wave models," in *8th International workshop on wave hindcasting and forecasting*, 2004.

[15] J. Aarnes and H. Krogstad, "Partitioning sequences for the dissection of directional ocean wave spectra: A review," Part of work package 4 (Wp4) of the EnviWave (EVG-2001-00017) research programme under the EU Energy, Environment and Sustainable Development programme, Tech. Rep., 2001.

[16] M. Tucker, P. G. Challenor, and C. D.J.T., "Numerical simulation of a random sea: a common error and its effect upon wave group statistics," *Applied Ocean Research*, vol. 5, pp. 118–122, 1984.

[17] J. Fitzgerald and L. Bergdahl, "Considering mooring cables for offshore wave energy converters," in *7th European Wave and Tidal energy Conference*, 2007.

[18] J. Fitzgerald, "Including moorings in the assessment of a generic offshore wave energy converter: A frequency domain approach." *Marine Structures*, vol. 21, pp. 23–46, 2008.

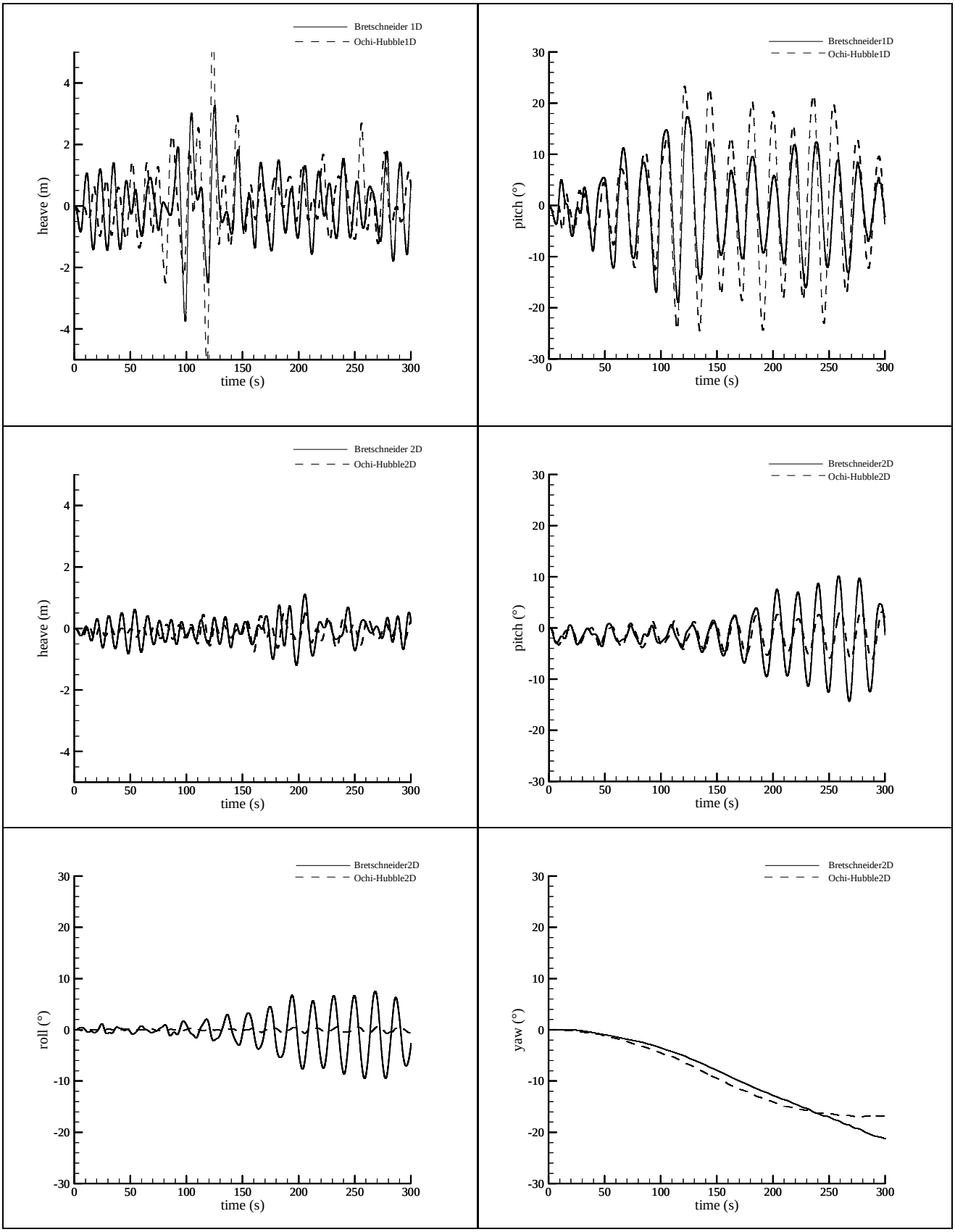

Figure 5: Heave, roll, pitch and yaw motion of the generic point absorber for the 1D and 2D Bretschneider and Ochi-Hubble spectra.

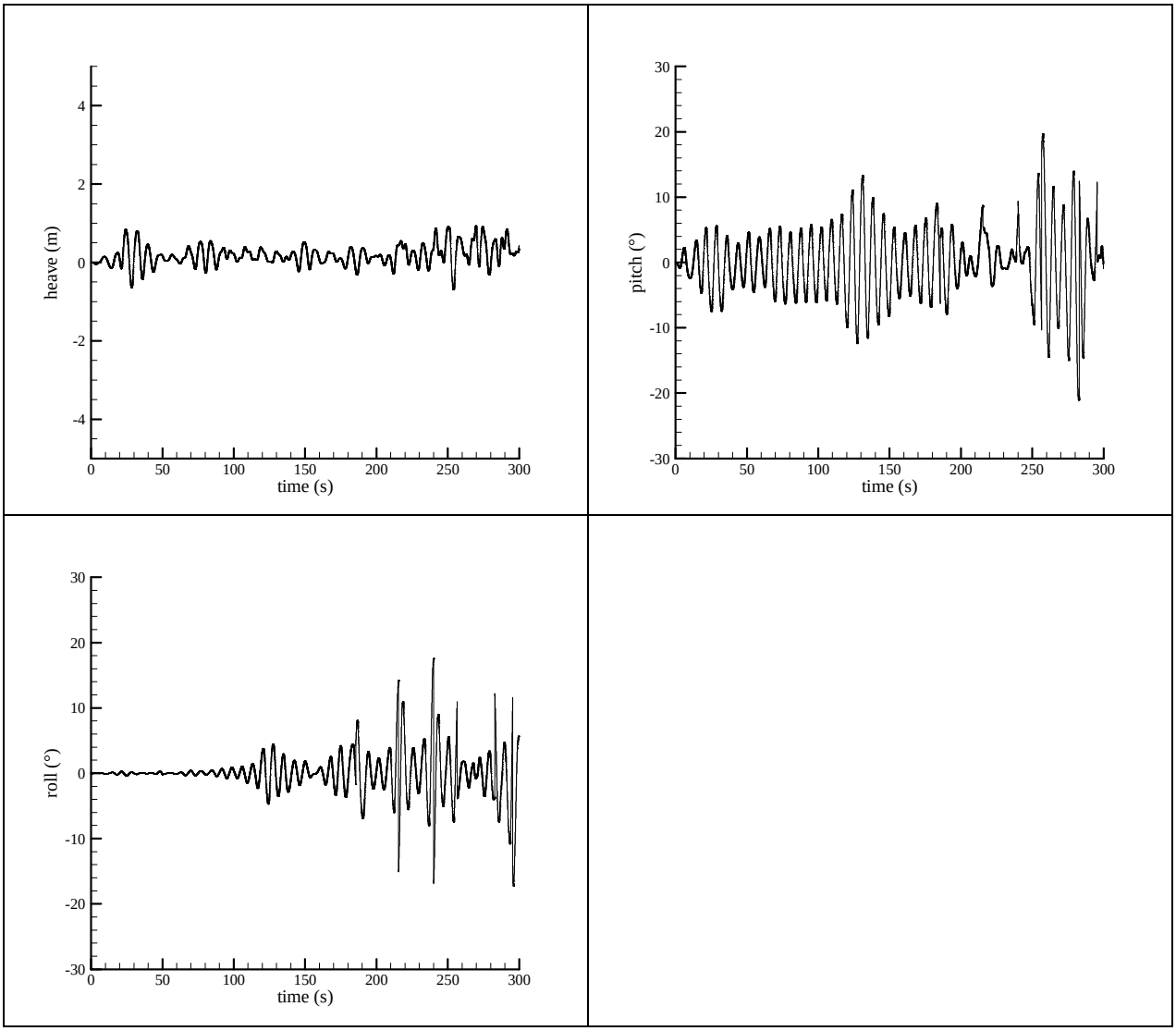

Figure 6: Heave, roll, pitch and yaw motion of the generic point absorber for the real 2D spectrum.